IEEE Access
Multidisciplinary | Rapid Review | Open Access Journal

Received February 5, 2019, accepted February 24, 2019, date of publication March 7, 2019, date of current version April 5, 2019.

Digital Object Identifier 10.1109/ACCESS.2019.2903409

Handover Skipping for LiFi

XIPING WU[1], (Member, IEEE), AND HARALD HAAS[2], (Fellow, IEEE)
[1]Department of Engineering Science University of Oxford, Oxford OX1 3PJ, U.K.
[2]LiFi Research and Development Centre, School of Engineering, The University of Edinburgh, Edinburgh EH9 3JL, U.K.

Corresponding author: Xiping Wu (xiping.wu@eng.ox.ac.uk)

This work was supported by the Engineering and Physical Sciences Research Council [Towards Ultimate Convergence of All Networks (TOUCAN)] under Grant EP/L020009/1. The work of H. Haas was supported by the EPSRC through the Established Career Fellowship under Grant EP/K008757/1.

ABSTRACT This paper studies handover skipping, which enables handovers between two non-adjacent access points (APs), in light fidelity (LiFi) networks. LiFi is an emerging wireless communication technology, which operates in a way similar to wireless fidelity (WiFi) but uses light waves as a medium. Compared with WiFi, LiFi has a relatively shorter range with a single AP. This could possibly cause more frequent handovers, and thus, handover skipping techniques are required. Conventional handover skipping methods rely on information about the user's trajectory, which is not ready to use at the AP. In this paper, a novel handover skipping scheme based on the reference signal received power (RSRP) is proposed. The new approach combines the value of RSRP and its rate of change to determine the handover target. Since RSRP is already used in the current handover schemes, the proposed method does not require additional feedback. The results show that compared with the standard handover scheme and the conventional handover skipping method, the proposed method can reduce handover rate by up to 29% and 17% and improve throughput by up to 66% and 26%, respectively.

INDEX TERMS Light fidelity (LiFi), visible light communication, handover skipping, received signal strength (RSS), reference signal received power (RSRP), user mobility, ultra-dense network.

I. INTRODUCTION

Global mobile data traffic will increase sevenfold between 2017 and 2022, with traffic from wireless fidelity (WiFi) and mobile devices accounting for 71 percent [2]. In 2022, there will be nearly 549 million public WiFi hotspots globally, up from 124 million hotspots in 2017. The high-density WiFi deployment would cause severe signal interference due to the limited spectrum resource of radio frequency (RF). To tackle the looming spectrum shortage in RF, wireless communication technologies based on extremely high frequencies have attracted significant attention, such as millimeter wave (mmWave) communications [3], massive multiple-input multiple-output (MIMO) [4], and visible light communications (VLC) [5]. The wireless networking use case of VLC is termed light-fidelity (LiFi) [6], which operates in a way similar to WiFi but uses light waves as a signal bearer. Unlike RF communications, LiFi access points (APs) can be integrated in the existing light infrastructure, e.g. light-emitting diode (LED) lamps, realizing a dual purpose system offering illumination and communication. Recent research shows that with a single off-the-shelf LED, LiFi is capable of achieving peak data rates above 10 Gbps [7]. Also, LiFi offers many other advantages over WiFi, including: i) a vast and licence-free spectrum; ii) secure communication as light does not penetrate opaque structures; and iii) availability in RF-restricted areas such as underwater and hospitals [8].

Due to inherently high propagation losses, all wireless communication technologies based on extremely high frequencies, including LiFi, have a relatively short range. Specifically, LiFi APs have a coverage area of approximately 2-3m in diameter [9]. This enables LiFi to achieve a very high area spectral efficiency through frequency reuse [10]. On the other hand, in such an ultra-dense network, the handover process becomes challenging mainly due to two issues: i) readily occurring ping-pong effects and ii) relatively short cell dwell time (CDT). Consequently, the signal strength strategy (SSS) method, which always chooses the AP providing the highest reference signal received power (RSRP), becomes hugely suboptimal for LiFi. In order to suppress the ping-pong effect, the standard handover scheme in long term evolution (LTE) [11] uses the idea of hysteresis, which prolongs the handover decision for a certain amount of time.

The associate editor coordinating the review of this manuscript and approving it for publication was Xiaofan He.

Nonetheless, this handover approach is not capable of tackling the second issue.

In order to avoid frequent handovers in the ultra-dense network, the concept of handover skipping was introduced [12]–[14]. A topology-aware skipping scheme was proposed in [12], by setting a pre-defined threshold to the chord length of the cell. A similar method was reported in [13], which extends the work to multi-AP association. Arshad *et al.* [14] developed a velocity-aware handover approach, which performs different skipping strategies according to the user's velocity, including: best connected, femto skipping, femto disregard and macro skipping. However, all of the above schemes rely on knowledge about the user's trajectory. As a result, they have the following limitations: i) the measurement of the user's trajectory is less accurate in an indoor scenario due to uncontrollable errors caused by multiple reflections on surfaces; and ii) extra feedback is needed to forward this information to the AP.

In this paper, an RSRP-based handover skipping method is proposed. The new method exploits the rate of change in RSRP to indicate whether a user is travelling towards the central area of the AP. Using a weighted average of the value of RSRP and its rate of change, the proposed method decides whether or not to skip a certain AP. Since the rate of change in RSRP is related to the user' velocity, the novel method is velocity-aware. Unlike the trajectory-based methods, the proposed approach does not need extra feedback as RSRP is already used in the standard handover scheme. For this reason, the proposed method can be readily implemented in practice. Mathematical expressions are derived to analyze the performance of the proposed method in terms of handover rate and coverage probability. In addition, the optimal weight coefficient is studied. Simulation results show that against the standard handover scheme and traditional handover skipping, the proposed approach can effectively decrease handover rate and increase user's throughput.

The remainder of this paper is organized as follows. In Section II, the system and channel models of an indoor LiFi network are described. The standard handover scheme of LTE is introduced in Section III. The novel handover skipping method is proposed in Section IV. In Section V, the handover rate and coverage probability of the proposed approach are theoretically analyzed. Simulation results are presented in Section VI. Finally, conclusions are drawn in Section VII.

II. SYSTEM MODEL

Consider an indoor optical wireless network consisting of a number of LiFi APs. The system is assumed to be a time division duplex. Each LiFi AP is integrated in a ceiling LED lamp, facing downwards. The APs employ different spectra and thus do not interfere with each other. A single photodiode (PD) pointing upwards is equipped at the receiver, which moves around the room following the random waypoint (RWP) model [15].

A LiFi channel is comprised of two components: line-of-sight (LoS) and non line-of-sight (NLoS) paths. Here

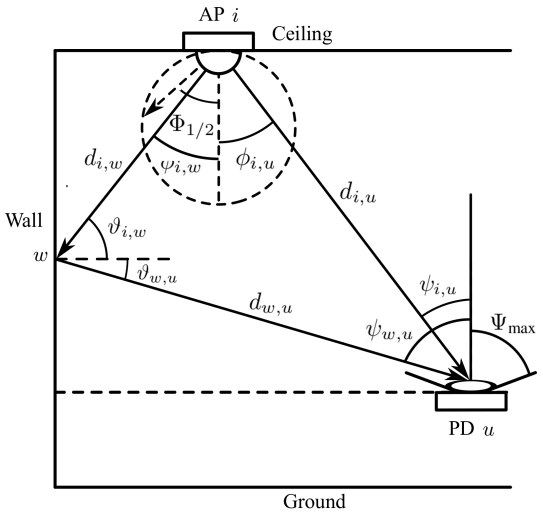

FIGURE 1. The LoS and first-order NLoS paths of the LiFi channel [17].

only first-order reflections are considered because second-order reflections typically contribute little [16]. Fig. 1 illustrates the LoS and first-order NLoS paths of the LiFi channel. Let i and u denote the AP and the user, respectively. The LoS path is the straight line between the AP and the user, and the corresponding Euclidean distance is denoted by $d_{i,u}$. Let $\phi_{i,u}$ and $\psi_{i,u}$ denote the angles of irradiance and incidence, respectively. The channel gain of LoS is represented by $H_{\text{LoS}}^{i,u}$, and it is given by [16, eq. (10)]:

$$H_{\text{LoS}}^{i,u} = \frac{(m+1)A_{\text{pd}}}{2\pi d_{i,u}^2} \cos^m(\phi_{i,u}) g_f g_c(\psi_{i,u}) \cos(\psi_{i,u}), \quad (1)$$

where $m = -\ln 2/\ln(\cos \Phi_{1/2})$ denotes the Lambertian emission order, and $\Phi_{1/2}$ is the angle of half intensity; A_{pd} is the physical area of the PD; g_f is the gain of the optical filter; the optical concentrator gain $g_c(\psi_{i,u})$ is given by [16, eq. (8)]:

$$g_c(\psi_{i,u}) = \begin{cases} \dfrac{n^2}{\sin^2(\Psi_{\max})}, & 0 \le \psi_{i,u} \le \Psi_{\max} \\ 0, & \psi_{i,u} > \Psi_{\max}, \end{cases} \quad (2)$$

where n stands for the refractive index, and $\Psi_{\max}$ represents the semi-angle of the field of view (FoV) of the PD.

A first-order reflection consists of two segments: i) from the AP to a small area w on the wall, and ii) from w to the user. The Euclidean distances of these two segments are denoted by $d_{i,w}$ and $d_{w,u}$. The angles of radiance and incidence regarding the first segment are $\phi_{i,w}$ and $\vartheta_{i,w}$, and for the second segment they are $\vartheta_{w,u}$ and $\psi_{w,u}$. The channel gain of NLoS is given by (3), as shown at the bottom of the next page, where A_w is the area of w and ρ_w denotes the wall reflectivity.

Adding (1) to (3), the total gain of the LiFi channel can be expressed as follows:

$$H_{\text{LiFi}}^{i,u} = H_{\text{LoS}}^{i,u} + H_{\text{NLoS}}^{i,u}. \quad (4)$$

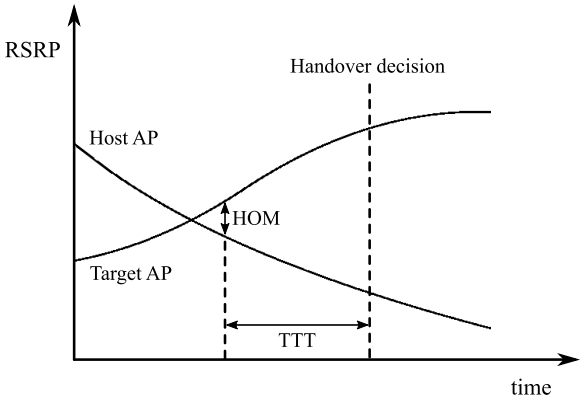

FIGURE 2. The handover scheme in LTE.

At the receiver, the PD converts the captured photons into an electric current:

$$I_{\text{elec}} = R_{\text{pd}} H_{\text{LiFi}}^{i,u} P_{\text{opt}}/\zeta, \tag{5}$$

where R_{pd} is the detector responsivity; P_{opt} is the transmitted optical power; and ζ denotes the ratio of P_{opt} to the optical signal power. The signal-to-noise ratio (SNR) of the user is denoted by $\gamma^{i,u}$, which can be written as follows:

$$\gamma^{i,u} = \frac{(R_{\text{pd}} H_{\text{LiFi}}^{i,u} P_{\text{opt}}/\zeta)^2}{N_{\text{LiFi}} B_{\text{LiFi}}}, \tag{6}$$

where N_{LiFi} denotes the power spectral density (PSD) of noise at the receiver, including shot noise and thermal noise, while B_{LiFi} is the bandwidth of the LiFi AP.

III. STANDARD HANDOVER SCHEME

In order to tackle the ping-pong effect, the handover scheme in LTE [11] introduces two parameters: handover margin (HOM) and time to trigger (TTT). Fig. 2 shows the principle of this standard handover scheme, which is referred to as STD in the rest of this paper. The RSRP of the host AP is denoted by P_{i_H}, and for the target AP it is P_{i_T}. Let δ_{HOM} denote the value of HOM. The STD scheme starts counting time when the following condition is met:

$$P_{i_T} > P_{i_H} + \delta_{\text{HOM}}. \tag{7}$$

The time counter continues as long as (7) is satisfied, and otherwise is reset. Let t_{TTT} denote the value of TTT. When the time counter reaches t_{TTT}, a handover decision is made to transfer the user from the host AP to the target one.

Fig. 3 exemplifies the movement paths of the user in a LiFi network. The STD scheme can guarantee a minimum connection time equal to t_{TTT}, which is usually limited to hundreds of milliseconds [11]. Thus, this scheme is able to avoid handovers to some APs the user crosses very quickly, e.g. Path 1. In this case, the user is directly transferred from

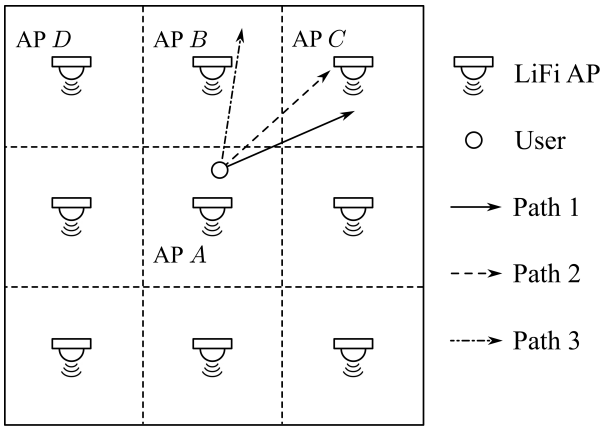

FIGURE 3. Different movement paths of the user in a LiFi network.

AP A to AP C, with AP B being skipped. However, the STD scheme cannot skip the APs where the user stays longer, even slightly, than t_{TTT}. Taking Path 2 for example, STD would handover the user from AP A to AP B, and then from AP B to AP C. Also, the user might experience random light-path blockages [18]. This can be deemed as an infinite attenuation for the link between the user and the blocked APs. The impact of random light-path blockages on handover rates will be studied in Section VI-E.

IV. PROPOSED HANDOVER SKIPPING METHOD

The value of RSRP reflects the distance between the AP and the user, and a higher RSRP signifies that the corresponding AP is closer to the user. For instance, when the user crosses the border between AP A and AP B in Fig. 3, AP B offers a higher RSRP than AP C. However, in Path 1 and Path 2, the user passes the outskirts of AP B and moves towards the central area of AP C. As a result, AP C provides a faster increase in RSRP than AP B. With respect to Path 3, the user moves towards the central area of AP B and thus gains a rapidly increasing RSRP from AP B. The RSRP and its rate of change can be used together to determine whether an AP needs to be skipped. The objective function of the target AP is denoted by Γ_i, and it is formulated as follows:

$$\Gamma_i = P_i^{(t_0)} + \lambda \Delta P_i, \tag{8}$$

where t_0 denotes the starting point of the time counter; $P_i^{(t_0)}$ is the RSRP of AP i at t_0; λ is a weight coefficient and its optimal value will be analyzed in Section VI-A; ΔP_i denotes the rate of change in RSRP, and it is expressed as:

$$\Delta P_i = \frac{P_i^{(t_0+t_{\text{TTT}})} - P_i^{(t_0)}}{t_{\text{TTT}}}. \tag{9}$$

Note that though straight-line movements are illustrated here, the proposed method is in fact applicable to

$$H_{\text{NLoS}}^{i,u} = \int_{A_w} \frac{(m+1)A_{\text{pd}}}{2(\pi d_{i,w} d_{w,u})^2} \rho_w \cos^m(\phi_{i,w}) g_f g_c(\psi_{w,u}) \cos(\psi_{w,u}) \cos(\vartheta_{i,w}) \cos(\vartheta_{w,u}) dA_w. \tag{3}$$

Algorithm 1 Proposed Handover Skipping Method

Input: $P_H^{(t)}, P_i^{(t)}, \forall i \in \mathcal{I}$
Output: i_T
  $t_c \Leftarrow 0$
  while $t_c < t_{\mathrm{TTT}}$ **do**
    if $P_i^{(t)} \leq P_H^{(t)} + \delta_{\mathrm{HOM}}, \forall i \in \mathcal{I}$ **then**
      $t_c \Leftarrow 0$
    else if $t_c = 0$ **then**
      $t_0 \Leftarrow t$
    else
      $t_c \Leftarrow t - t_0$
    end if
    $t \Leftarrow t + 1$
  end while
  $\Gamma_i \Leftarrow P_i^{(t_0)} + \lambda \left(P_i^{(t_0+t_{\mathrm{TTT}})} - P_i^{(t_0)} \right) / t_{\mathrm{TTT}}$
  $i_T \Leftarrow \max\{\Gamma_i\}$

random movements. This is because the user's movement can be approximated in a straight line for a short period t_{TTT}. The proposed scheme starts counting time in a way similar to STD. When the time counter reaches t_{TTT}, the AP with the largest Γ_i is chosen to be the target AP. It is worth noting that the target AP does not have to be the one triggering the time counter. In Fig. 3, for example, AP B excites the time counter but the target AP could be AP C. At the end of the time counter, a handover will be made immediately if the target AP already meets the condition in (7). Otherwise, the handover will be stalled until the target AP meets the condition. During this period, the target AP might be recalculated if the user alters its moving direction or speed.

The parameter $P_i^{(t_0)}$ in (8) depends on the position of the point that the user crosses the border, whereas ΔP_i reflects the direction and speed of the user's movement. If the crossing point is very close to the border between two candidate APs (e.g. AP B and AP C in Path 1), the RSRP offered by them would be almost the same. In this case, ΔP_i is the dominant factor to determine the target AP. On the contrary, the values of RSRP significantly differ when the crossing point is far away from one candidate AP, e.g. AP C in Path 3. Thus, $P_i^{(t_0)}$ becomes the dominant factor. As for Path 2, AP B provides an RSRP marginally higher than AP C. Meanwhile, the ΔP_i of AP C increases with the user's speed. If the user moves fast, it is handed over from AP A to AP C, with AP B being skipped. Otherwise, the user is transferred to AP B due to the insignificant influence of ΔP_i. This shows that the proposed approach is adaptive to the user's velocity. Let $\mathcal{I}$ denote the set of all candidate APs. The output of the time counter is denoted by t_c. The pseudo code of the proposed handover skipping method is given in Algorithm 1.

V. THEORETICAL ANALYSIS OF HANDOVER SKIPPING PERFORMANCE

In this section, the theoretical performance of the proposed handover skipping method is analyzed for an arbitrary line trajectory. The area covered by the LiFi network is assumed to be boundless. As a result, only LoS paths need to be taken into account.

A. HANDOVER RATE

First, we analyze the handover rate of the SSS method, where there is no handover skip. We focus on the square deployment of LiFi APs as it is commonly used in practice to provide uniform illumination. The handover rate with the Poisson point process (PPP) deployment can be found in [19]. It is assumed that the user enters the coverage area of an AP at an arbitrary point, called an entry point, with an arbitrary angle θ. The distance between the entry point and a reference point is denoted by δ, as shown in Fig. 11. Let r denote the length of the side of the coverage area. The length of the user's movement path inside the coverage area is denoted by d_{path}. The average value of d_{path} is represented by $\bar{d}_{\mathrm{path}}$, which is derived in Appendix A. The handover rate equals the user's speed v divided by $\bar{d}_{\mathrm{path}}$. The handover rate of SSS, denoted by η, can be calculated as follow:

$$\eta = \frac{\pi v}{r} \left[3 \log \left(\sqrt{2} + 1 \right) + 1 - \sqrt{2} \right]^{-1}. \tag{10}$$

Then we derive the probability of handover skipping. With the proposed method, the user skips an AP when another AP exists providing a larger Γ_i. This event is denoted by X and its probability $\mathbb{P}(X)$ can be expressed as follows:

$$\mathbb{P}(X) = 1 - \mathbb{P}(\neg X), \tag{11}$$

where:

$$\mathbb{P}(\neg X) = \mathbb{P}(\Gamma_B \geq \Gamma_i, \forall i, i \neq B). \tag{12}$$

The host AP borders 8 neighbors with the square deployment. Further APs are unlikely to become the handover target due to the much lower RSRP they provide. Let's consider the case that the user leaves AP A and enters AP B, as shown in Fig. 3. AP C and AP D are the only possible candidates for handover skipping, as compared to the remaining neighbors which perform worse in terms of both P and ΔP. Since the square deployment is axisymmetric, we assume that the user crosses the right half segment of the border between AP A and AP B. The candidate for handover skipping could only be AP C if θ is less than 90Âř, and otherwise AP D. Therefore, $\mathbb{P}(\neg X)$ can be rewritten as:

$$\mathbb{P}(\neg X) = \int_{\delta=0}^{r/2} \mathbb{P}(\neg X \mid \delta) \mathbb{P}(\delta) d\delta, \tag{13}$$

where $\mathbb{P}(\neg X \mid \delta)$ is given in (14), as shown at the bottom of the next page.

See the expressions of $\mathbb{P}(\Gamma_B \geq \Gamma_C \mid \theta, \delta)$ and $\mathbb{P}(\Gamma_B \geq \Gamma_D \mid \theta, \delta)$ in Appendix B. Since θ is uniformly distributed between 0 and π, the above equation can be rewritten as:

$$\mathbb{P}(\neg X \mid \delta) = \frac{\Theta_D(\delta) - \Theta_C(\delta)}{\pi}. \tag{15}$$

As δ is uniformly distributed between 0 and $\frac{r}{2}$, we have $\mathbb{P}(\delta) = \frac{2}{r}$. Therefore, (13) can be computed as follows:

$$\mathbb{P}(\neg X) = \frac{2}{\pi r} \int_{\delta=0}^{r/2} [\Theta_D(\delta) - \Theta_C(\delta)]\, d\delta. \tag{16}$$

The handover rate of the proposed method is denoted by η_{HS}, which is the product of η and $\mathbb{P}(\neg X)$. Combining (10) and (16), η_{HS} can be expressed as (17), as shown at the bottom of this page.

B. COVERAGE PROBABILITY

The coverage probability is defined as the probability that the user's SNR is above a certain threshold γ_T. This threshold corresponds to a certain horizontal distance between the user and the AP, which is denoted by l_T. According to (6), l_T can be computed as follows:

$$l_T = \sqrt{\left[\frac{(m+1)A_{\mathrm{pd}}h^{m+1}g_f g_c R_{\mathrm{pd}} P_{\mathrm{opt}}}{2\pi\zeta\sqrt{\gamma_T N_{\mathrm{LiFi}} B_{\mathrm{LiFi}}}}\right]^{\frac{2}{m+3}} - h^2} \tag{18}$$

The user's SNR is larger than γ_T when $l < l_T$. Therefore, the coverage probability of the SSS method is equal to $\mathbb{P}(l < l_T)$. Assuming the user is randomly located in the square coverage area with an equal probability, $\mathbb{P}(l < l_T)$ can be expressed as (19), shown at the bottom of this page.

It can be found that the coverage probability of the SSS method depends on the size of the coverage area, and is thus denoted by $\mathcal{P}(r)$. Regarding the proposed method, its coverage probability is equal to $\mathcal{P}(r)$ when no handover skip occurs. When there is a handover skip, the distance between the host and target APs changes from r to $\sqrt{2}r$. The coverage probability of the proposed method can be estimated as follows:

$$\mathcal{P}_{\mathrm{HS}}(r) = \mathbb{P}(\neg X)\mathcal{P}(r) + \mathbb{P}(X)\mathcal{P}(\sqrt{2}r). \tag{20}$$

However, the skipped AP is located at one end-point of the border between the host and target APs, making this corner area unlikely to be involved in handover skipping. Therefore, (20) would underestimate the user's SNR in the lower end. More details will be given in the following context.

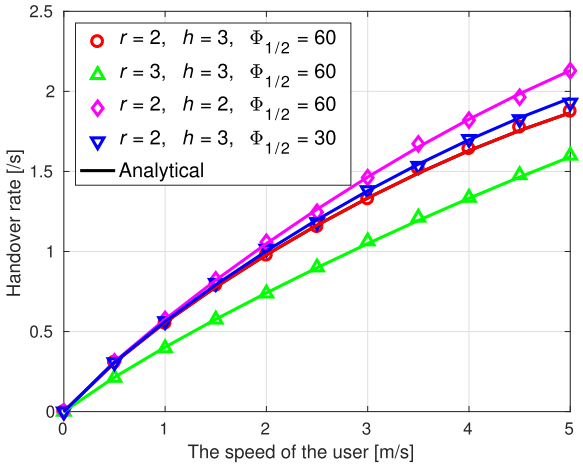

FIGURE 4. Handover rate versus the user's speed.

C. VALIDATION

Monte Carol simulations are conducted to verify the above theoretical analysis. Here the weight λ is fixed to be 1. In Fig. 4, the handover rate is shown as a function of the user's speed. As can be seen, the analytical results in (17) closely match the simulations. Also, the handover rate decreases when: i) the distance between the nearest APs increases; or ii) the vertical distance between the user and the AP increases; or iii) the half-intensity angle of the LED increases.

Taking $v = 5$ m/s as an example, Fig. 5 presents the coverage probability of the proposed method. The impact of the user's speed will be studied in the following section. In general, the estimated expression agrees with the simulations. In the region of lower SNRs, the analytical results are below the simulations with a marginal gap, as explained. Also, it can be found that the three situations stated in the previous paragraph all result in a decrease in SNR. This concludes that the handover rate can be reduced at the cost of a decreased SNR.

$$\mathbb{P}(\neg X \mid \delta) = \int_{\theta=0}^{\pi/2} \mathbb{P}(\Gamma_B \geq \Gamma_C \mid \theta, \delta)\mathbb{P}(\theta)d\theta + \int_{\theta=\pi/2}^{\pi} \mathbb{P}(\Gamma_B \geq \Gamma_D \mid \theta, \delta)\mathbb{P}(\theta)d\theta. \tag{14}$$

$$\eta_{\mathrm{HS}} = \frac{2v}{r^2}\left[3\log\left(\sqrt{2}+1\right) + 1 - \sqrt{2}\right]^{-1} \int_{\delta=0}^{r/2} [\Theta_D(\delta) - \Theta_C(\delta)]\, d\delta. \tag{17}$$

$$\mathbb{P}(l < l_T) = \begin{cases} \pi\left(\frac{l_T}{r}\right)^2, & l_T \leq \frac{r}{2} \\ 2\sqrt{\left(\frac{l_T}{r}\right)^2 - \frac{1}{4}} + \left(\frac{l_T}{r}\right)^2\left[\pi - 4\arccos\left(\frac{r}{2l_T}\right)\right], & \frac{r}{2} < l_T < \frac{\sqrt{2}r}{2} \\ 1, & l_T \geq \frac{\sqrt{2}r}{2}. \end{cases} \tag{19}$$

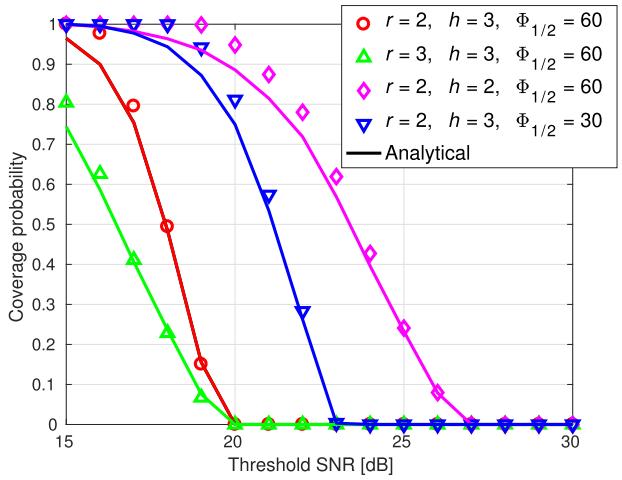

FIGURE 5. Coverage probability versus threshold SNR.

TABLE 1. Simulation parameters.

Parameter	Value
Room size (length by width by height)	8m × 8m × 3m
The physical area of the PD, A_{pd}	1 cm^2
The gain of the optical filter, g_f	1
Refractive index, n	1.5
Half-intensity radiation angle, $\Phi_{1/2}$	60°
FoV semi-angle of the PD, $\Psi_{\max}$	90°
Transmitted optical power, P_{opt}	3 Watt
The ratio of P_{opt} to the optical signal power, ζ	3
Detector responsivity, R_{pd}	0.53 A/W
Wall reflectivity, ρ_w	0.8
Bandwidth per LiFi AP, B_{LiFi}	200 MHz
PSD of noise in LiFi, N_{LiFi}	10^{-21} A^2/Hz
Handover overhead	200 ms [20]

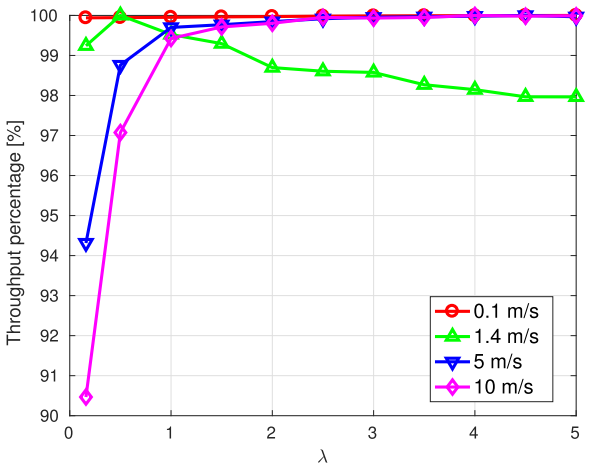

FIGURE 6. Throughput versus the weight coefficient.

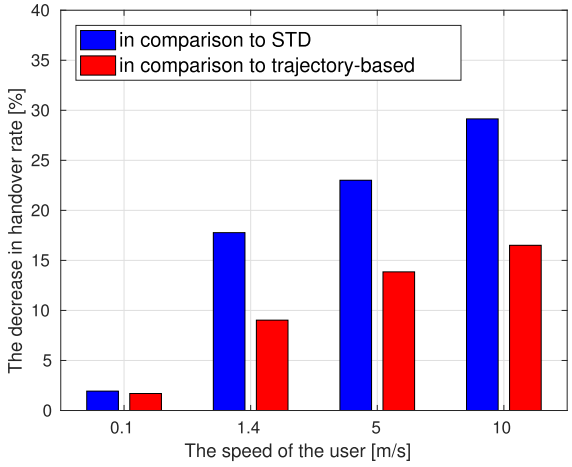

FIGURE 7. The decrease in handover rate versus the user's speed.

VI. SIMULATION RESULTS

In this section, Monte Carlo simulations are carried out to evaluate the performance of the proposed method. The STD and the trajectory-based handover skipping method in [12] are considered as benchmarks. In order to provide a fair comparison, the three methods employ the same HOM and TTT, which are set to be 1 dB and 160 ms [11]. In addition, we consider 16 LiFi APs, with the separation between the two nearest APs being fixed to be 2m. Other required parameters are summarized in Table 1.

A. THE IMPACT OF THE WEIGHT COEFFICIENT

First, we study the effect of λ on the performance of the proposed method. Note that λ needs to be larger than t_{TTT}, as stated in Lemma 2. Four movement scenarios are considered: 0.1 m/s (slow moving), 1.4 m/s (walking), 5 m/s (running) and 10 m/s (sprinting). As shown in Fig. 6, for a slow moving user, the throughput almost remains the same when λ varies in the displayed range. This is because in this case, the rate of change in RSRP is negligible when determining the handover target. As the user's speed increases to 1.4 m/s, choosing a proper λ becomes crucial. On the one hand, a too small λ would disable the function of handover skipping. On the other hand, a too large λ would cause unnecessary handover skipping. For a fast moving user, the throughput is a monotonically increasing function of λ in the displayed range. The reason for this is that the rate of change in RSRP becomes the dominant factor. Considering the optimal solutions to different speeds of the user, λ is set to be 1 in the following analysis.

B. HANDOVER RATE

Second, the handover rate performance of the proposed scheme is evaluated. Fig. 7 shows the decreases in handover rate when the proposed approach is compared with STD and the trajectory-based method. Two outcomes are observed: i) compared to the baseline methods, the proposed scheme can effectively decrease the handover rate for different speeds of the user; and ii) as the user's speed increases, the decrease in handover rate becomes larger. At $v = 0.1$ m/s, the proposed method achieves a handover rate merely 2% less than STD. When v increases to 1.4 m/s, this gap increases to 18%. For $v = 10$ m/s, the proposed approach reduces the handover rate by 29% against STD, and by 17% in comparison to the trajectory-based method.

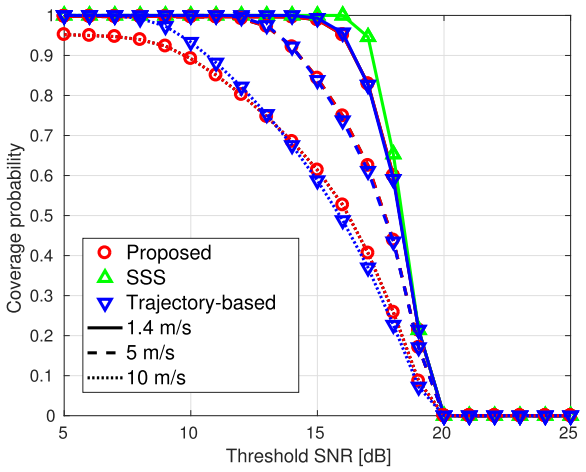

FIGURE 8. Coverage probability for different speeds of the user.

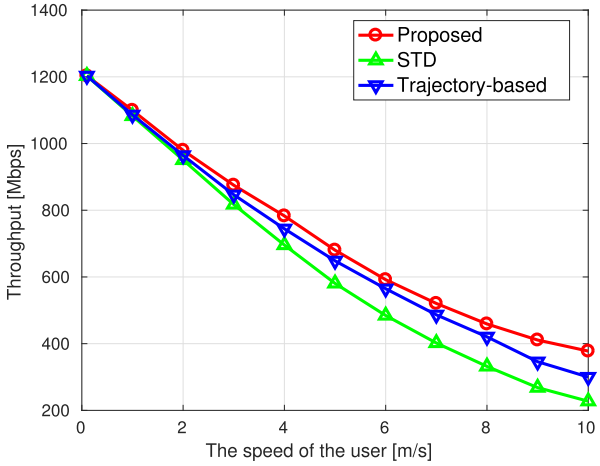

FIGURE 9. Throughput versus the user's speed.

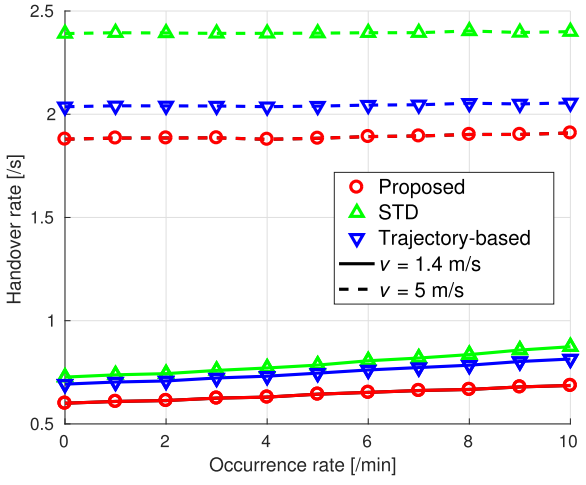

FIGURE 10. Handover rate versus the occurrence rate.

C. COVERAGE PROBABILITY

Third, the coverage probability for different speeds of the user in presented in Fig. 8. Here SSS is considered as a baseline, because its host AP only depends on the user's location, regardless of the user's speed. This method can be deemed as a special case of STD with zero HOM and TTT. As shown, the coverage probability of the proposed scheme decreases as the user's speed increases, especially for medium SNRs between 14 and 18 dB. High SNRs correspond to cell centers, where handover skips rarely occur; low SNRs correspond to cell corners, where the target AP of handover skipping can provide a comparable SNR against the skipped AP. Otherwise, the SNR performance would substantially decrease when a handover skip occurs. Nonetheless, at the 50-th percentile, the SNR of the proposed approach is only 2 dB less than that of SSS. This means that with the proposed method, the user can achieve an SNR comparable to that of SSS in at least 50% situations. Also, it is observed that at $v = 10$ m/s, there is a noticeable gap between the coverage probabilities of the proposed method and the trajectory-based method at lower SNRs. This is because when the user moves very fast, the proposed scheme might skip more than one AP, leading to a significant decrease in SNR.

D. THROUGHPUT

The user's throughput, measured by the modulation and coding scheme in [21], is shown in Fig. 9 as a function of the user's speed. No data transmission is counted during the handover process. As shown, the proposed approach always achieves a higher throughput than the baseline methods. This gain becomes more significant as the user's speed increases. For $v = 5$ m/s, the proposed method can improve throughput over STD and the trajectory-based method by 17% and 5%. When the user's speed increases to 10 m/s, the corresponding gains increase to 66% and 26%, respectively.

E. THE IMPACT OF RANDOM LIGHT-PATH BLOCKAGES

Finally, we study the impact of random light-path blockages on handover rates. In queueing theory [22], the Poisson point process is widely used to model random events such as the arrival of packages at a switch. Here the events of light-path blockages are also assumed to follow the Poisson distribution, and the mean is termed the occurrence rate. As shown in Fig. 10, the handover rates of all involved methods noticeably increase with the occurrence rate in the case of $v = 1.4$ m/s. While the user's speed increases to 5 m/s, the handover rates are hardly affected by the change in the occurrence rate. This is because for fast moving users, in comparison to user mobility, the random light-path blockage is an insignificant factor that affects the handover process.

VII. CONCLUSION

In this paper, a novel handover skipping approach was proposed for LiFi networks. Unlike the conventional method using information about the user's trajectory, the proposed scheme is based on RSRP, a parameter commonly used in present handover algorithms. Thus, the proposed method does not require extra feedback and can be readily implemented in realistic systems. Specifically, the rate of change in RSRP is employed to suggest whether the user is moving towards an AP. A weighted average of this parameter and RSRP itself is used to determine the target AP for handover.

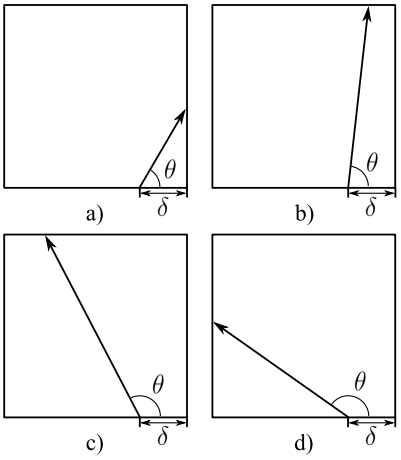

FIGURE 11. The movement paths of the user in the coverage area of an AP.

Also, the handover rate and coverage probability of the proposed scheme are mathematically derived. Furthermore, the effects of the weight coefficient on the performance of the proposed scheme are analyzed. Results show that the proposed approach can greatly reduce the handover rate against STD, especially when the user is moving relatively fast. Regarding the system throughput, the proposed method outperforms STD and the trajectory-based handover skipping method by up to 66% and 26%, respectively. Future research will involve hybrid LiFi and WiFi networks and study the resulting change in the performance of handover skipping.

APPENDIX

A. DERIVATION OF $\bar{d}_{path}$

For a certain entry point, there are four types of possible paths, as shown in Fig. 11. Each type corresponds to a mathematical expression of $d_{\text{path}}(\delta)$:

$$d_{\text{path}}(\delta)=\begin{cases}\dfrac{\delta}{\cos(\theta)}, & 0\le\theta<\theta_1\\ \dfrac{r}{\sin(\theta)}, & \theta_1\le\theta<\dfrac{\pi}{2}\\ \dfrac{r}{\sin(\pi-\theta)}, & \dfrac{\pi}{2}\le\theta<\theta_2\\ \dfrac{r-\delta}{\cos(\pi-\theta)}, & \theta_2\le\theta\le\pi,\end{cases}\tag{21}$$

where:

$$\begin{cases}\theta_1=\arctan\left(\dfrac{r}{\delta}\right)\\ \theta_2=\pi-\arctan\left(\dfrac{r}{r-\delta}\right).\end{cases}\tag{22}$$

Since $\sin(\pi-\theta)=\sin(\theta)$, the second and third types can be merged into one. The average value of $d_{\text{path}}(\delta)$ is then calculated by (23), as shown at the bottom of this page. The integrals on the right side of (23) can be solved by calculating the antiderivatives. Consequently, (23) can be rewritten as (24), as shown at the bottom of this page, where:

$$\begin{cases}\delta_1=\sqrt{\delta^2+r^2}\\ \delta_2=\sqrt{(r-\delta)^2+r^2}.\end{cases}\tag{25}$$

With δ varying from 0 to $\frac{r}{2}$, the parameter $\bar{d}_{\text{path}}$ is computed as follows:

$$\bar{d}_{\text{path}}=\frac{2}{r}\int_{\delta=0}^{\frac{r}{2}}\bar{d}_{\text{path}}(\delta)d\delta.\tag{26}$$

Substituting (24) into (26), $\bar{d}_{\text{path}}$ can be expressed as:

$$\bar{d}_{\text{path}}=\frac{r}{\pi}\left[3\log\left(\sqrt{2}+1\right)+1-\sqrt{2}\right].\tag{27}$$

B. DERIVATION OF $\mathbb{P}(\Gamma_B\ge\Gamma_C\mid\theta,\delta)$ AND $\mathbb{P}(\Gamma_B\ge\Gamma_D\mid\theta,\delta)$

According to (1), (5) and (8), Γ_i can be written as follows:

$$\Gamma_i=g_{\text{eff}}\left[\left(1-\frac{\lambda}{t_{\text{TTT}}}\right)\mathcal{P}_i^{(t_0)}+\frac{\lambda}{t_{\text{TTT}}}\mathcal{P}_i^{(t_0+t_{\text{TTT}})}\right],\tag{28}$$

where:

$$g_{\text{eff}}=\left[\frac{(m+1)A_{\text{pd}}g_f g_c R_{\text{pd}}P_{\text{opt}}}{2\pi\zeta}\right]^2\left(h_{i,u}^{(t)}\right)^{2m+2},\tag{29}$$

and:

$$\mathcal{P}_i^{(t)}=\left[\left(h_{i,u}^{(t)}\right)^2+\left(l_{i,u}^{(t)}\right)^2\right]^{-m-3},\tag{30}$$

where $h_{i,u}^{(t)}$ and $l_{i,u}^{(t)}$ denote the vertical and horizontal distances between AP i and user u, respectively. Since all APs are assumed to sit on the same level, $h_{i,u}^{(t)}$ is a constant and thus can be abbreviated to h.

Removing the common items in Γ_B and Γ_C, the item $\mathbb{P}(\Gamma_B\ge\Gamma_C\mid\theta,\delta)$ can be rewritten as:

$$\mathbb{P}(\Gamma_B\ge\Gamma_C\mid\theta,\delta)=\mathbb{P}(Z(\theta)\ge0\mid\theta,\delta),\tag{31}$$

where $Z(\theta)$ is expressed as (32), shown at the bottom of the next page. Given δ and θ, we have (33), as shown at the bottom of the next page.

Lemma 1: For $\theta\in\left[0,\frac{\pi}{2}\right]$, $Z(\theta)$ increases monotonically if $\mathcal{P}_B^{(t_0+t_{\text{TTT}})}-\mathcal{P}_C^{(t_0+t_{\text{TTT}})}\ge0$. Otherwise, $Z(\theta)$ decreases monotonically first and then increases monotonically.

Proof: Note that the item $\left(1-\frac{\lambda}{t_{\text{TTT}}}\right)\left(\mathcal{P}_B^{(t_0)}-\mathcal{P}_C^{(t_0)}\right)$ in (32) is a constant with respect to θ. Therefore, $Z(\theta)$ changes with $\left(\mathcal{P}_B^{(t_0+t_{\text{TTT}})}-\mathcal{P}_C^{(t_0+t_{\text{TTT}})}\right)$, which is denoted by $F(\theta)$.

$$\bar{d}_{\text{path}}(\delta)=\frac{1}{\pi}\left(\int_{\theta=0}^{\theta_1}\frac{\delta}{\cos(\theta)}d\theta+\int_{\theta=\theta_1}^{\theta_2}\frac{r}{\sin(\theta)}d\theta+\int_{\theta=\theta_2}^{\pi}\frac{\delta-r}{\cos(\theta)}d\theta\right).\tag{23}$$

$$\bar{d}_{\text{path}}(\delta)=\frac{1}{\pi}\left[\delta\log\left(\frac{r+\delta_1}{\delta}\right)+r\log\left(\frac{\delta+\delta_1}{\delta_2-r+\delta}\right)+(r-\delta)\log\left(\frac{r+\delta_2}{r-\delta}\right)\right].\tag{24}$$

Let $F_1(\theta)$ and $F_2(\theta)$ denote $\left(l_{B,u}^{(t_0+t_{\mathrm{TTT}})}\right)^2$ and $\left(l_{C,u}^{(t_0+t_{\mathrm{TTT}})}\right)^2$, respectively. The derivative of $F_1(\theta)$ and $F_2(\theta)$ are computed as follows:

$$\begin{cases} F_1'(\theta) = vt_{\mathrm{TTT}}\left[(2\delta - r)\sin(\theta) - r\cos(\theta)\right] \\ F_2'(\theta) = vt_{\mathrm{TTT}}\left[(2\delta + r)\sin(\theta) - r\cos(\theta)\right]. \end{cases} \tag{34}$$

For $\delta \in \left(0, \frac{r}{2}\right)$, we have $2\delta - r < 0$. In addition, since $\theta \in \left[0, \frac{\pi}{2}\right]$, $\sin(\theta)$ and $\cos(\theta)$ are non-negative and cannot be zeros at the same time. Thus $F_1'(\theta)$ is always negative. Note that $m > 0$ for all possible $\Phi_{1/2}$. Hence, $\mathcal{P}_B^{(t_0+t_{\mathrm{TTT}})}$ increases monotonically. As for $F_2'(\theta)$, its derivative $F_2''(\theta)$ is expressed as follows:

$$F_2''(\theta) = vt_{\mathrm{TTT}}\left[(2\delta + r)\cos(\theta) + r\sin(\theta)\right]. \tag{35}$$

The parameter $F_2''(\theta)$ is always positive. Also, we have $F_2'(0) = -vt_{\mathrm{TTT}}r < 0$ and $F_2'(\frac{\pi}{2}) = vt_{\mathrm{TTT}}(2\delta + r) > 0$. Thus there exists one and only one θ meeting $F_2'(\theta) = 0$. This signifies that $\mathcal{P}_C^{(t_0+t_{\mathrm{TTT}})}$ monotonically increases until $F_2'(\theta) = 0$ and then monotonically decreases. Note that $F_2'(\theta)$ is always larger than $F_1'(\theta)$. In other words, $\mathcal{P}_B^{(t_0+t_{\mathrm{TTT}})}$ has a larger slope than $\mathcal{P}_C^{(t_0+t_{\mathrm{TTT}})}$ when $\mathcal{P}_B^{(t_0+t_{\mathrm{TTT}})}$ and $\mathcal{P}_C^{(t_0+t_{\mathrm{TTT}})}$ are both increasing. As a result, $F(\theta)$ monotonically increases if $F(0) \geq 0$. Otherwise, $F(\theta)$ monotonically decreases first and then monotonically increases. ∎

Lemma 2: For $\theta \in \left[0, \frac{\pi}{2}\right]$, there is up to one solution to $Z(\theta) = 0$ on condition that $\lambda > t_{\mathrm{TTT}}$.

Proof: According to Lemma 1, $Z(\theta)$ monotonically increases when $F(0) \geq 0$. It is evident that Lemma 2 is true in this case. When $F(0) < 0$, $Z(\theta)$ monotonically decreases first and then monotonically increases. In this case, Lemma 2 is true if $Z(0) < 0$. Substituting $\theta = 0$ into (32), we have:

$$Z(0) = \left(1 - \frac{\lambda}{t_{\mathrm{TTT}}}\right)\left(\mathcal{P}_B^{(t_0)} - \mathcal{P}_C^{(t_0)}\right) + \frac{\lambda}{t_{\mathrm{TTT}}}F(0). \tag{36}$$

Note that $\mathcal{P}_B^{(t_0)} - \mathcal{P}_C^{(t_0)}$ is always non-negative and $\frac{\lambda}{t_{\mathrm{TTT}}}$ is assumed to be larger than 1. Hence $Z(0) < 0$ when $F(0) < 0$. ∎

The parameter t_{TTT} is very small in practice, with a typical value of 0.16 s [11]. Therefore, the condition $\lambda > t_{\mathrm{TTT}}$ can be readily satisfied. This is also a guideline for the choice of λ.

Lemma 3: There exists at least one θ to meet $Z(\theta) \geq 0$.

Proof: Substituting $\theta = \dfrac{\pi}{2}$ into (32), we have:

$$Z\left(\tfrac{\pi}{2}\right) = \left(1 - \frac{\lambda}{t_{\mathrm{TTT}}}\right)\left(\mathcal{P}_B^{(t_0)} - \mathcal{P}_C^{(t_0)}\right) + \frac{\lambda}{t_{\mathrm{TTT}}}F\left(\tfrac{\pi}{2}\right). \tag{37}$$

The derivative of $Z\left(\frac{\pi}{2}\right)$ with respect to l is written as (38), shown at the bottom of this page, where F_A, F_B, F_C and F_D are given by (39), as shown at the bottom of this page.

As aforementioned, t_{TTT} is very small. In practice, we have $0 \leq vt_{\mathrm{TTT}} < r$ and thus $\left(\frac{r}{2}\right)^2 \geq \left(\frac{r}{2} - vt_{\mathrm{TTT}}\right)^2$. Hence, $F_C \geq F_A$ and $F_D \geq F_B$, leading to $F_C + F_D - F_A - F_B \geq 0$. Also, it is evident that $F_A + F_B > 0$. Thus the derivative of $Z\left(\frac{\pi}{2}\right)$ with respect to δ is always positive. In other words, $Z\left(\frac{\pi}{2}\right)$ monotonically increases with δ. Meanwhile, $Z\left(\frac{\pi}{2}\right) = 0$ when $\delta = 0$. Therefore, $Z\left(\frac{\pi}{2}\right)$ must be non-negative. ∎

Combining the three above lemmas, there is one and only one θ to satisfy $Z(\theta) = 0$ when $F(0) < 0$. For $F(0) \geq 0$, $Z(\theta)$

$$Z(\theta) = \left(1 - \frac{\lambda}{t_{\mathrm{TTT}}}\right)\left(\mathcal{P}_B^{(t_0)} - \mathcal{P}_C^{(t_0)}\right) + \frac{\lambda}{t_{\mathrm{TTT}}}\left(\mathcal{P}_B^{(t_0+t_{\mathrm{TTT}})} - \mathcal{P}_C^{(t_0+t_{\mathrm{TTT}})}\right). \tag{32}$$

$$\begin{cases} l_{B,u}^{(t_0)} = \sqrt{\left(\frac{r}{2}\right)^2 + \left(\frac{r}{2} - \delta\right)^2} \\ l_{B,u}^{(t_0+t_{\mathrm{TTT}})} = \sqrt{\left(\frac{r}{2} - vt_{\mathrm{TTT}}\sin(\theta)\right)^2 + \left(\frac{r}{2} - \delta + vt_{\mathrm{TTT}}\cos(\theta)\right)^2} \\ l_{C,u}^{(t_0)} = \sqrt{\left(\frac{r}{2}\right)^2 + \left(\frac{r}{2} + \delta\right)^2} \\ l_{C,u}^{(t_0+t_{\mathrm{TTT}})} = \sqrt{\left(\frac{r}{2} - vt_{\mathrm{TTT}}\sin(\theta)\right)^2 + \left(\frac{r}{2} + \delta - vt_{\mathrm{TTT}}\cos(\theta)\right)^2}. \end{cases} \tag{33}$$

$$\frac{dZ\left(\frac{\pi}{2}\right)}{dl} = 2(m+3)\left[F_A + F_B + \frac{\lambda}{t_{\mathrm{TTT}}}\left(F_C + F_D - F_A - F_B\right)\right], \tag{38}$$

$$\begin{cases} F_A = \left(\frac{r}{2} + \delta\right)\left[h^2 + \left(\frac{r}{2}\right)^2 + \left(\frac{r}{2} + \delta\right)^2\right]^{-m-4} \\ F_B = \left(\frac{r}{2} - \delta\right)\left[h^2 + \left(\frac{r}{2}\right)^2 + \left(\frac{r}{2} - \delta\right)^2\right]^{-m-4} \\ F_C = \left(\frac{r}{2} + \delta\right)\left[h^2 + \left(\frac{r}{2} - vt_{\mathrm{TTT}}\right)^2 + \left(\frac{r}{2} + \delta\right)^2\right]^{-m-4} \\ F_D = \left(\frac{r}{2} - \delta\right)\left[h^2 + \left(\frac{r}{2} - vt_{\mathrm{TTT}}\right)^2 + \left(\frac{r}{2} - \delta\right)^2\right]^{-m-4}. \end{cases} \tag{39}$$

would always be positive if there does not exist a solution to $Z(\theta) = 0$. Unfortunately, due to the high order of the polynomial in (32), it is difficult to derive a closed-form solution to $Z(\theta) = 0$. Let Θ_C denote this solution if there exists one and otherwise $\Theta_C = 0$. Then $\mathbb{P}(\Gamma_B \geq \Gamma_C \mid \theta, \delta)$ can be computed as follows:

$$\mathbb{P}(\Gamma_B \geq \Gamma_C \mid \theta, \delta) = \begin{cases} 0, & 0 \leq \theta < \Theta_C \\ 1, & \Theta_C \leq \theta \leq \dfrac{\pi}{2}. \end{cases} \tag{40}$$

Similarly, $\mathbb{P}(\Gamma_B \geq \Gamma_D \mid \theta, \delta)$ can be expressed as follows:

$$\mathbb{P}(\Gamma_B \geq \Gamma_D \mid \theta, \delta) = \begin{cases} 1, & \dfrac{\pi}{2} < \theta \leq \Theta_D \\ 0, & \Theta_D < \theta \leq \pi, \end{cases} \tag{41}$$

where Θ_D is the solution to $\Gamma_B = \Gamma_D$ if there exists one, and otherwise $\Theta_D = \pi$.

ACKNOWLEDGEMENT

This paper was presented in part at the IEEE VTC Spring 2019 [1].

REFERENCES

[1] X. Wu and H. Haas, "RSS-based handover skipping for ultra-dense attocell networks," in *Proc. IEEE 89th Veh. Technol. Conf. (VTC Spring)*, Kuala Lumpur, Malaysia, 2019, pp. 1–5.
[2] *Cisco Visual Networking Index: Forecast and Trends, 2017–2022*, Cisco, San Jose, CA, USA, Nov. 2018.
[3] T. S. Rappaport *et al.*, "Millimeter wave mobile communications for 5G cellular: It will work!" *IEEE Access*, vol. 1, pp. 335–349, May 2013.
[4] H. Q. Ngo, A. Ashikhmin, H. Yang, E. G. Larsson, and T. L. Marzetta, "Cell-free massive MIMO versus small cells," *IEEE Trans. Wireless Commun.*, vol. 16, no. 3, pp. 1834–1850, Mar. 2017.
[5] H. Burchardt, N. Serafimovski, D. Tsonev, S. Videv, and H. Haas, "VLC: Beyond point-to-point communication," *IEEE Commun. Mag.*, vol. 52, no. 7, pp. 98–105, Jul. 2014.
[6] H. Haas, L. Yin, Y. Wang, and C. Chen, "What is LiFi?" *J. Lightw. Technol.*, vol. 34, no. 6, pp. 1533–1544, Mar. 15, 2016.
[7] M. Islim *et al.*, "Towards 10 Gb/s orthogonal frequency division multiplexing-based visible light communication using a GaN violet micro-LED," *Photon. Res.*, vol. 5, no. 2, pp. A35–A43, Apr. 2017.
[8] L. Hanzo, H. Haas, S. Imre, D. O'Brien, M. Rupp, and L. Gyongyosi, "Wireless myths, realities, and futures: From 3G/4G to optical and quantum wireless," *Proc. IEEE*, vol. 100, pp. 1853–1888, May 2012.
[9] H. Haas, "Visible light communication," in *Proc. Opt. Fiber Commun. Conf. Exhib. (OFC)*, Los Angeles, CA, USA, 2015, pp. 1–72.
[10] I. Stefan, H. Burchardt, and H. Haas, "Area spectral efficiency performance comparison between VLC and RF femtocell networks," in *Proc. IEEE Int. Conf. Commun. (ICC)*, Budapest, Hungary, Jun. 2013, pp. 3825–3829.
[11] *LTE; Evolved Universal Terrestrial Radio Access (E-UTRA); Radio Resource Control (RCC); Protocol Specification (Release 13)*, document TS 36.331 v13.0.0., 3GPP, Valbonne, France, Jan. 2016.
[12] R. Arshad, H. Elsawy, S. Sorour, T. Y. Al-Naffouri, and M.-S. Alouini, "Handover management in 5G and beyond: A topology aware skipping approach," *IEEE Access*, vol. 4, pp. 9073–9081, 2016.
[13] E. Demarchou, C. Psomas, and I. Krikidis, "Mobility management in ultra-dense networks: Handover skipping techniques," *IEEE Access*, vol. 6, pp. 11921–11930, 2018.
[14] R. Arshad, H. ElSawy, S. Sorour, T. Y. Al-Naffouri, and M.-S. Alouini, "Velocity-aware handover management in two-tier cellular networks," *IEEE Trans. Wireless Commun.*, vol. 16, no. 3, pp. 1851–1867, Mar. 2017.
[15] D. B. Johnson and D. A. Maltz, "Dynamic source routing in ad hoc wireless networks," *Mobile Computing*, 1996, pp. 153–181.
[16] J. M. Kahn and J. R. Barry, "Wireless infrared communications," *Proc. IEEE*, vol. 85, no. 2, pp. 265–298, Feb. 1997.
[17] X. Wu, M. Safari, and H. Haas, "Access point selection for hybrid Li-Fi and Wi-Fi networks," *IEEE Trans. Commun.*, vol. 65, no. 12, pp. 5375–5385, Dec. 2017.
[18] X. Wu and H. Haas, "Access point assignment in hybrid LiFi and WiFi networks in consideration of LiFi channel blockage," in *Proc. IEEE 18th Int. Workshop Signal Process. Adv. Wireless Commun. (SPAWC)*, Sapporo, Japan, Jul. 2017, pp. 1–5.
[19] W. Bao and B. Liang, "Stochastic geometric analysis of handoffs in user-centric cooperative wireless networks," in *Proc. IEEE 35th Annu. Int. Conf. Comput. Commun. (INFOCOM)*, San Francisco, CA, USA, Apr. 2016, pp. 1–9.
[20] J. Xiao and F. Liu, "A pre-scanning fast handoff scheme for VoIP in WLANs," *Int. J. Future Comput. Commun.*, vol. 8, no. 2, pp. 343–354, 2015.
[21] *IEEE Standard for Information Technology—Local and Metropolitan Area Networks—Specific Requirements—Part 11: Wireless LAN Medium Access Control (MAC) and Physical Layer (PHY) Specifications Amendment 5: Enhancements for Higher Throughput*, IEEE Standard 802.11n-2009, Oct. 2009, pp. 1–565.
[22] L. Kleinrock, *Queueing Systems: Theory*. West Sussex, U.K.: Wiley, 1976.

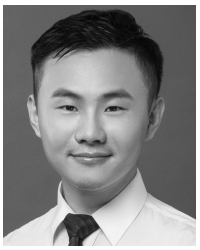

XIPING WU (S'11–M'14) received the B.Sc. degree from Southeast University, China, in 2008, and the M.Sc. and Ph.D. degrees from The University of Edinburgh, U.K., in 2011 and 2015, respectively. From 2011 to 2014, he was a Marie-Curie Early-Stage Researcher, funded by the European Union's Seventh Framework Program (FP7). From 2013 to 2014, he was on secondment to the Department of Electrical and Information Engineering, University of L'Aquila, Italy. From 2014 to 2018, he held a Postdoctoral Fellowship with The University of Edinburgh, funded by the British Engineering and Physical Sciences Research Council. He is currently a Research Associate with the Department of Engineering Science, University of Oxford. His main research interests include wireless communication theory, visible light communication, and wireless network management.

HARALD HAAS (S'98–A'00–M'03–SM'16–F'17) received the Ph.D. degree from The University of Edinburgh, in 2001. He is currently with the Chair of Mobile Communications, The University of Edinburgh, and the Founder and the Chief Scientific Officer with pureLiFi Ltd., and also the Director of the LiFi Research and Development Center, The University of Edinburgh. He has authored or co-authored over 400 conference and journal papers, including a paper in science. He was co-authored a book *Principles of LED Light Communications Towards Networked Li-Fi* (Cambridge University Press, 2015). His main research interests include optical wireless communications, hybrid optical wireless and RF communications, spatial modulation, and interference management in wireless networks. He first introduced and coined spatial modulation and LiFi. LiFi was listed among the 50 best inventions in the TIME Magazine 2011. He was an invited speaker at TED Global 2011. His talk, Wireless Data from Every Light Bulb, has been watched online over 2.5 million times. He gave a second TED Global talk, in 2015, on the use of solar cells as LiFi data detectors and energy harvesters. This has been viewed online over 2.0 million times. He was elected as a Fellow of the Royal Society of Edinburgh, in 2017. He was a co-recipient of recent best paper awards from VTC-Fall 2013, VTC-Spring 2015, ICC 2016, and ICC 2017, the EURASIP Best Paper Award for the *Journal on Wireless Communications and Networking*, in 2015, and the Jack Neubauer Memorial Award from the IEEE Vehicular Technology Society. In 2012 and 2017, he was a recipient of the prestigious Established Career Fellowship from the Engineering and Physical Sciences Research Council (EPSRC). In 2014, he was selected by EPSRC as one of ten Recognizing Inspirational Scientists and Engineers Leaders in U.K. In 2016, he received the Outstanding Achievement Award from the International Solid State Lighting Alliance. He is an Associate Editor of the IEEE/OSA JOURNAL OF LIGHTWAVE TECHNOLOGIES.